LASER
& PHOTONICS
REVIEWS

Laser Photonics Rev. **9,** No. 1, 98–104 (2015) / **DOI** 10.1002/lpor.201400133

ORIGINAL
PAPER

Abstract This contribution presents an optofluidic droplet router which is able to route and steer microdroplets using optically induced forces created solely by the bulk photovoltaic effect on a nonlinear substrate. The combination of microfluidic tools with the properties of a photorefractive crystal allows for the generation of dielectrophoretic forces that can be either repulsive, leading to *virtual barriers*, or attractive, creating *virtual rails*. The sign of these forces is solely determined by the electrical properties of the liquid medium under investigation. Moreover, the induced structures on the bottom of the microfluidic channel are optically reconfigurable, so that the same device can easily be adopted for different purposes. Appropriate droplet-generating devices are fabricated by UV illumination of SU-8 and polydimethylsiloxane replica molding of the master structures. The bottom of the channels is formed by an iron-doped lithium niobate crystal, whose internal electric fields are induced by structured illumination patterns and exert dielectrophoretic forces on droplets in the microfluidic section.

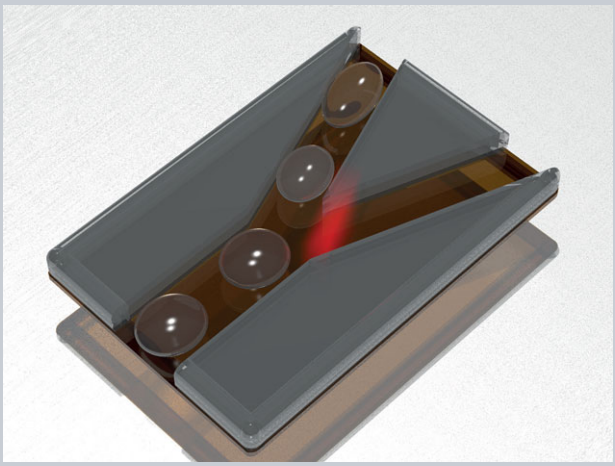

Optofluidic droplet router

Michael Esseling[1,*], Annamaria Zaltron[1,2], Wolfgang Horn[3], and Cornelia Denz[1]

1. Introduction

Droplets, as the discretized units of otherwise continuous fluid media, are of particular interest in the world of microfluidics, since they enable new concepts and fabrication techniques in physical, biological, and chemical sciences. Droplet-based microfluidic systems, also known as *digital microfluidics*, allow transferring mixing or synthesis experiments to the micrometer scale, thus reducing both reagent volumes and reaction times. Potential applications include the manipulation and analysis of single bacteria [1] and the continuous and controlled synthesis of semiconducting nanoparticles [2], polymer microparticles of various shapes [3], or Janus particles with two separate sides that feature different optical and electrical properties [4, 5]. In these devices, the ability to actuate droplets is fundamental. Various active and passive techniques have been proposed up to now to manipulate discrete droplets for relevant operations such as mixing, sorting, reaction, and sensing of discrete droplets [6, 7]. However, these manipulation techniques often rely on a fixed structure with little possibility to adapt to new manipulation scenarios without changing the device. A solution is provided by the use of optofluidics. This field holds the promise of enabling novel devices by the fusion and mutual interaction of optics and microfluidics. It includes the manipulation of light by liquid media, such as in liquid–liquid (L^2) waveguides [8, 9], but also the opposite direction, where optical or optically induced forces actuate fluids [10] or liquid constituents are detected by optical methods [11].

In particular, the present contribution demonstrates a flexible method of manipulating microfluidic droplets only by means of light-induced dielectrophoresis (DEP), completely realized on a photorefractive crystal substrate. DEP describes a phenomenon in which strongly modulated electric fields polarize and attract or repel dielectric matter [12]. Since its first description in the 1950s, DEP has been used to sort cells or actuate flows, either in a fixed electrode configuration [13–16] or flexibly switched by light, resulting in optically induced DEP or *optoelectronic tweezers* [17–19], which connect fluidics with the optical world. Recently, it was demonstrated that DEP also occurs on the surface of a photorefractive lithium niobate ($LiNbO_3$) crystal [20], as a consequence of a structured illumination which gives rise to strong electric fields inside the material. Owing to these light-induced electric fields, which penetrate also the volume outside the crystal, dielectrophoretic and electrophoretic forces have been used for particle trapping in air [21–23], and also in microfluidic surroundings [24]. To the best of our knowledge, this paper describes the first use of a photorefractive $LiNbO_3$ crystal as an active bottom layer to route droplets in a microfluidic droplet generator. The movement of droplets and bubbles generated inside the microfluidic channel is influenced by dielectrophoretic forces from virtual electrodes, which are created through appropriate, arbitrarily configurable illumination of the

[1] Nonlinear Photonics Group, Institute of Applied Physics, University of Münster, Corrensstrasse 2/4, 48149, Münster, Germany
[2] Physics and Astronomy Department, University of Padova, via Marzolo 8, 35131, Padova, Italy
[3] Nonlinear Optical Lithography Group, Institute of Applied Physics, University of Münster, Corrensstrasse 2/4, 48149, Münster, Germany
*Corresponding author: e-mail: michael.esseling@uni-muenster.de

underlying $LiNbO_3$ substrate. This original approach enables the realization of two-dimensional structures that are adaptable merely by changing the illumination pattern. The use of $LiNbO_3$ provides a unique material for the bottom substrate that is chemically highly resistant due to its crystalline nature and able to generate high electric fields without any external electrodes. It is therefore highly suited for microfluidic integration and can easily complement or replace glass substrates in a multitude of droplet formation devices.

This paper is structured in the following way. Firstly, the physical origin of the light-induced forces that create virtual rails or barriers is explained. The following sections describe the production of droplet generators by femtosecond laser ablation and replica molding as well as the active, nonlinear iron-doped $LiNbO_3$ substrate that transforms the incident illumination pattern into electric field distributions. Subsequently, the assembly of the optofluidic droplet routing device is described and first routing scenarios are demonstrated and discussed.

2. Dielectrophoretic forces and liquid selection

The effect used for the manipulation of droplets is the fundamental effect of *dielectrophoresis*. It was demonstrated in the 1950s by Pohl [12] that strongly inhomogeneous fields induce a significant polarization inside a dielectric material, which experiences different magnitudes of electrophoretic forces on both ends of the induced dipole. The resulting net forces either attract particles to or repel them from regions of high field intensity. The magnitude of the force on a dielectric sphere can be calculated as [25]

$$F_{\mathrm{DEP}} = 2\pi r^3 \varepsilon_{\mathrm{m}} \varepsilon_0 K(\omega) \nabla E^2 \,, \tag{1}$$

where r is the particle radius, ε_{m} the relative permittivity of the surrounding medium, ε_0 the vacuum permittivity, E the electric field, and $K(\omega)$ the frequency-dependent Clausius–Mossotti factor, which for small frequencies ω, such as those occurring on $LiNbO_3$ substrates [24], simplifies to the contrast between the conductivities σ_{p} and σ_{m} of particle p and surrounding medium m, respectively [25]:

$$K(\omega \to 0) = \frac{\sigma_{\mathrm{p}} - \sigma_{\mathrm{m}}}{\sigma_{\mathrm{p}} + 2\sigma_{\mathrm{m}}} \,. \tag{2}$$

However, in the current application, the fluid medium under investigation can hardly be described as a small spherical particle. Therefore a different model that describes the fluid as a collection of infinitely small dipoles with dipole moment $\vec{p}$ is more suitable [26]. The total force is derived by calculating an integral over the *Kelvin polarization force density*, i.e. all dipoles in the fluid volume [27]

$$\vec{F} = \int (N_{\mathrm{p}} \vec{p}) \nabla E \mathrm{d}V = \frac{1}{2} \varepsilon_0 \int (\varepsilon_{\mathrm{l}} - \varepsilon_{\mathrm{m}}) \nabla E^2 \mathrm{d}V \,, \tag{3}$$

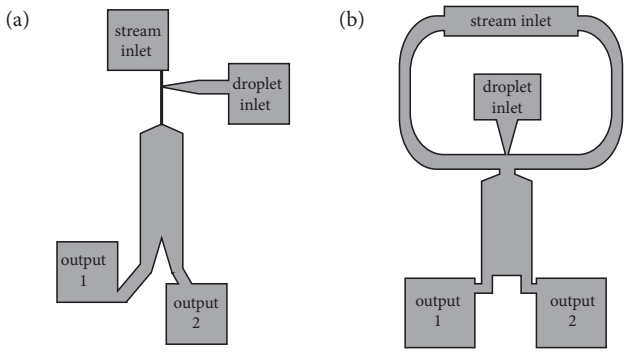

Figure 1 (a) T-channel junction and (b) collinear flow-focusing droplet generators used in this contribution; see text for details.

where N_{p} describes the volume density of individual dipoles with dipole moment $\vec{p}$ and $(\varepsilon_{\mathrm{l}} - \varepsilon_{\mathrm{m}})$ is the excess polarization of a liquid l surrounded by another medium m [28]. In either description of Eqs. (1) and (3), the force is attractive if the droplet possesses a higher conductivity/permittivity than that of the surrounding medium and vice versa. Thereby, electric field gradients can be used to deflect droplets in a microfluidic device by light-induced *virtual barriers* or to guide them on *virtual rails*. The two main constituents of such a device are the microfluidic channels, where droplets are generated, and the bottom material sealing the channel, which provides the electric field to manipulate the droplets. A suitable combination of fluids is selected, so that one medium is less conductive and less polarizable than the other. For example, in the case of Novec hydrofluorether (3M, St Paul, MN) droplets flowing freely in tetradecane (TD), the Novec 7300/7500 fluids are more polarizable, with $\varepsilon_{\mathrm{TD}} \approx 2$ and $\varepsilon_{7300/7500} = 6.14/5.83$ [29,30], as well as more conducting, with $\sigma_{7300/7500} = 5.6 \times 10^{-12}/4.5 \times 10^{-9}$ S cm^{-1} [29, 30] being much larger than $\sigma_{\mathrm{TD}} \leq 1 \times 10^{-15}$ S cm^{-1} (own measurement). It is therefore a safe assumption that even in the case of comparably large droplets, the forces acting on droplets suspended in a base medium will be attractive for Novec droplets in TD and repulsive if air or another less polarizable bubble is immersed in Novec fluid.

3. Droplet generators

In order to demonstrate the light-induced actuation capabilities of the $LiNbO_3$ substrate, an integrated droplet-producing device has to be assembled in order to bring the droplets into close contact with the active bottom substrate. Droplet generation requires two immiscible fluids, one of them being a low-volume stream which is injected into a high-volume base stream. Two different generator geometries were used (Fig. 1), the first being a T-junction geometry, where the base stream is intersected by a droplet nozzle, so that droplets are cut off from the nozzle [31]. This geometry has the advantage of being fairly easy to implement and allowing a straightforward change of the

ratio between droplets and base liquids by changing the flow speeds. However, due to the production of the droplets in immediate contact with the channel, they have a tendency to stick to the channel walls, even if the channel gets broader (Fig. 1). The adhesion forces can become comparable to the strength of the dielectrophoretic forces, which impedes droplet manipulation. The second design that can circumvent the problem of sticking droplets is a collinear or *flow-focusing* geometry. Three streams flow collinearly, with the base streams flowing at a higher flow rate, so that the middle stream is effectively segmented into discrete droplets [32]. It has the advantage that the droplets are free-flowing and ideally do not have contact with the channel walls. In order to economize as regards additional pumps, the base stream is split up into two to arrive at the droplet nozzle from both sides. Although such a simplified setup does not allow the independent control of the two sides of the flow, it was found that droplets were still produced with only little bias to either side. In any case, the implementation of more pumping devices to allow for even better droplet control is straightforward and independent of the presented manipulation technique.

For each geometry, illumination masks were fabricated by femtosecond laser ablation of aluminum from sputter-coated glass slides. Using these masks, SU-8 masters for polydimethylsiloxane (PDMS) replica molding were fabricated by UV illumination with a 405 nm laser. The SU-8 was spin-coated onto glass substrates to a thickness of 65 μm. The preprocessing and the developing of the SU-8 masters were carried out following the usual procedures described in the literature [33–35]. It should be noted, however, that after developing, the SU-8 masters were post-baked at 150°C for 1 hour, which significantly increased the adhesion of SU-8 to the glass substrate. The PDMS mixture was degassed prior to the casting process, then poured into the mold and cured at 100°C for 45 minutes. The casting mold further consisted of a metal frame with threads, to which the microfluidic tubing was attached. During the experiments the microfluidic flows were driven by PSD/3 micropumps (Duratec Analysetechnik, Hockenheim, Germany).

4. Virtual electrodes on iron-doped lithium niobate (Fe:$LiNbO_3$)

The electric fields responsible for droplet manipulation originate from the $LiNbO_3$ substrate by which the PDMS channels are sealed. $LiNbO_3$ is a photorefractive material, which upon inhomogeneous light illumination produces strongly modulated internal space-charge fields. The main mechanism of this phenomenon is the bulk photovoltaic effect [36], which describes the unilateral movement of photo-excited charge carriers in the substrate, mainly along its optical axis $\hat{z}$. This charge migration leads to a net charge separation between dark and bright areas, which in turn gives rise to the so-called space-charge electric field [37]. Since the photorefractive performance of the material strongly depends on the concentration of donor and acceptor atoms, $LiNbO_3$ crystals are often doped with transition metals, such as iron in the present case. In $LiNbO_3$, the iron dopant atoms are present in two valence states, Fe^{2+} and Fe^{3+}, which act as donor and acceptor of free charges, respectively. In this way the sensitivity is increased in the visible region and very high internal fields of up to 10^7 V m^{-1} can be created [38].

Table 1 List of Fe:$LiNbO_3$ crystals used in the experiments reported in this contribution.

	sample	$c_{Fe^{2+}}/c_{Fe^{3+}}$	size (mm)
as-grown	AT2	0.039	$15 \times 10 \times 2$
reduced	151.7	0.74	$13.5 \times 10 \times 0.6$

The Fe:$LiNbO_3$ crystals used in the study described here were grown at the University of Padua according to the protocol described in [39]. The crystals used for the experiments must fulfill two criteria: first, they should be fast so that virtual electrodes can be induced in a reasonable time frame; second, and even more important, the internal space-charge fields E_{sc} should be high enough to enable the efficient manipulation of droplets and bubbles. The one-center model [40], which describes the time evolution and magnitude of light-induced internal electric fields in Fe:$LiNbO_3$, predicts a linear increase of the photoconductivity, hence the writing speed, with the degree of reduction r, i.e. the ratio between the concentration of filled (Fe^{2+}) and empty (Fe^{3+}) traps. This ratio can be adjusted using the thermal treatment described in [39]. However, it was found in a previous study [39] that for degrees of reduction higher than unity, the saturation field, which enters quadratically in Eq. (1), decreases disproportionately. Therefore, to ensure that the electric fields are sufficiently high, a crystal with intermediate degree of reduction of $r = 0.74$ was used, if not stated otherwise (see Table 1). To compare performances, a commercial as-grown crystal was used in a single experiment. Although the saturation field for the as-grown crystal was twice as high as for the reduced one, 3.79×10^7 and 1.85×10^7 V m^{-1}, respectively [39], no significant qualitative difference in the dielectrophoretic forces could be observed in these experiments. This is most likely due to the fact that the as-grown crystal has a degree of reduction of $r \approx 0.039$, and therefore it is almost 20 times slower and so the saturation value of the electric field is never actually reached in the time scale of our experiments [39]. Therefore, the best sample for this experiment is the reduced one since it allows a quicker induction and erasure of the light-induced structures, as is shown later.

5. Integrated optofluidic droplet router device

The combination of the PDMS droplet generator with the active $LiNbO_3$ layer forms the droplet router device. Before sealing the microfluidic circuit with the $LiNbO_3$ substrate, the former was subjected to a UV treatment for

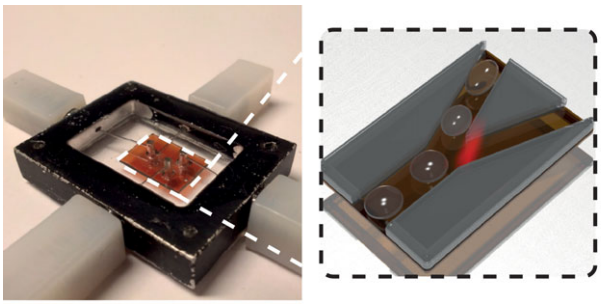

Figure 2 Photograph of the assembled droplet generator device, sealed by the 151.7 photorefractive crystal, and a magnified sketch of a virtual barrier (red), deflecting bubbles by negative DEP.

20 minutes to improve the adhesion of the crystal to the PDMS and to render it hydrophilic, which markedly reduces swelling when brought into contact with apolar solvents, such as TD [41]. The metal frame (Fig. 2) comprising the connectors for tubing is integrated into a commercial Nikon TE2000U microscope, which allows monitoring of the movements of the droplets in the microfluidic channel and creation of electric fields in the underlying Fe:$LiNbO_3$ crystal at the same time. In order to induce virtual barriers or rails in the bottom of the channel, a 532 nm laser illuminates a high-resolution amplitude spatial light modulator (ASLM; HES 6001, Holoeye, Berlin, Germany). The ASLM turns the polarization of the incoming light pixelwise, and a polarizer transfers the polarization pattern into an amplitude pattern. This pattern is demagnified and imaged to the sample plane. A dichroic mirror in the filter revolver separates the high-intensity green light for the induction of the internal space-charge field from the incandescent white light for observation.

6. Droplet switch and splitter

The prepared device can be used for a multitude of applications, where the sign of the force only depends on the electric properties of the fluids and the geometry of the underlying virtual electrodes can be arbitrarily chosen by changing the illumination pattern on the ASLM. For example, a droplet or gas bubble can be routed by closing an outlet with a repulsive light-induced electrode.

Figure 3 shows the results of a droplet deflection experiment conducted in the T-channel droplet generator sealed by the reduced $LiNbO_3$ sample. Air bubbles are generated in a Novec 7500 flow. The flow ratio between base and flow layer in this experiment was adjusted to be 4:1. As explained previously, droplets or bubbles in this geometry have a tendency to stick to the side walls of the channel, which results in bubbles exiting the device to the right outlet prior to the induction of *virtual barriers*. Since air inherently has both a lower conductivity and dielectric permittivity than Novec 7500 fluid, the forces generated by an electric field gradient will be repulsive. Figure 3a shows that without any

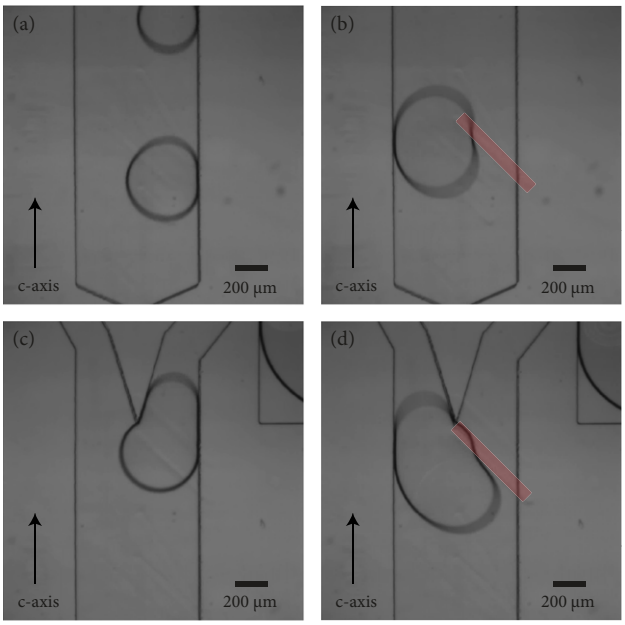

Figure 3 Air bubble removal by virtual electrodes. Without any modification of the substrate, air bubbles travel along the channel undisturbed (a), but can be steered around certain areas by introducing virtual barriers (red) in the $LiNbO_3$ substrate (b); initially, droplets exit through the right port (c); after the induction of a binary stripe, this exit is reliably closed by negative dielectrophoretic forces (d). (see video 1: barrierForAirBubbles.avi, in online supporting information)

modification of the substrate air bubbles flow towards the exit sticking to the right side of the channel. After writing a binary stripe pattern at $I = 0.56$ W cm^{-2} for 12 s, the bubbles are removed from the wall and are routed around the barrier (Fig. 3b). Furthermore, the initial exit port of the bubbles can be completely closed by a repulsive electrode written with the same parameters (Fig. 3c,d). Of course, the repulsive force acts not only to the side but also upwards. However, the air bubbles cannot travel *over* the virtual barrier due to the small height of the microchannel of 65 μm. The high photorefractive phase retardation in the crystal makes the virtual electrode partly visible even in bright field illumination (Figs. 3 and 4). The incident intensity of the writing beam may seem large at first, but considering that the total size of the barrier is small, the total power necessary for its inscription is only 0.14 mW. Since the time constant for the induction of electric fields in $LiNbO_3$ is known to be inversely proportional to the incident light intensity [40], a more efficient light modulation or use of a laser with higher power can significantly reduce the writing time. As a further advantage of the material, it should be noted that, due to the low dark conductivity of the $LiNbO_3$ crystal, a light-induced electric field remains even when the laser illumination is switched off, so that the induced optical routing path persists for an extended amount of time [42]. In our experiments, a decrease in the repulsive force could be observed approximately 60 s after the green laser had been switched off. In contrast to other trapping experiments,

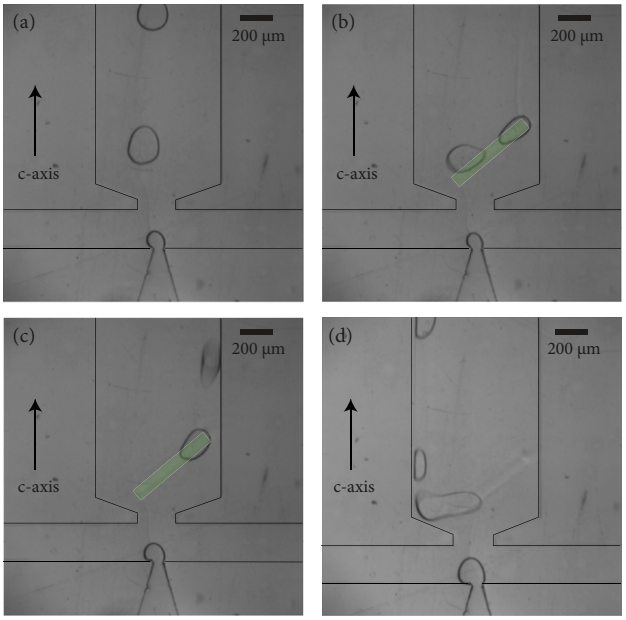

Figure 4 Droplet routing on *virtual rails* (highlighted by green lines). On the unmodified 151.7 substrate, droplets of Novec 7300 in a collinear stream of TD flow freely towards the exit (a). After the induction of *virtual rails* on the crystal surface, the positive dielectrophoretic forces guide the Novec droplets towards the right-hand exit port, where they are immobilized at the end of rails (b) until released by the next droplet (c). The virtual rails can be erased with the microscope illumination lamp, after which the droplets flow to the left (d). Although the virtual rails were erased near the surface in (d), they are still partly visible due to the refractive index modification in the volume. Note that due to the low refractive index difference between TD and PDMS, the borders of the channel have been highlighted by dark lines. (see video 2: virtualRails_for_NovecDroplets.avi, in online supporting information)

where dielectric matter was trapped in surrounding air, the discharge of the internal field in our setup occurs not by the dark conductivity of the crystal, which is negligibly low, but primarily through the finite conductivity of the liquid medium flowing over the surface, so the discharge time is highly dependent on the media conductivities.

By an appropriate selection of materials, it is also possible to generate forces acting in the opposite direction. Figure 4 shows the case where positive dielectrophoretic forces were employed. Droplets of Novec 7300 were generated in the collinear flow droplet device in a base stream of TD. The flow rates for a reliable generation of droplets were 5 μL min^{-1} for the TD base flow and 0.4 μL min^{-1} for the Novec 7300 droplet infusion. Since the conductivity as well as the dielectric permittivity of Novec 7300 are larger than those of TD, both the Clausius–Mossotti factor as well as the excess polarization are positive, implying that the Novec droplets are attracted by electric field gradients. Therefore, the previous virtual barriers become *virtual rails* on which droplets are guided. The virtual rail was inscribed into the $LiNbO_3$ crystal at an intensity of 0.4 W cm^{-2} for approximately 15 s. Before the appearance of the electric fields on the $LiNbO_3$ substrate, the droplets are flowing freely towards the exit ports, remaining almost in the middle of the channel (Fig. 4a). After the inscription of the virtual rail, droplets at the flow-focusing nozzle follow the induced field gradient and are directed to the right-hand exit port (Fig. 4b). Moreover, if the droplet reaching the virtual rail is not too large, it can even be completely immobilized by the strong attractive forces. In this case, the retaining force must equal or even exceed the drag force. If two droplets of the same volume coagulate, the drag force becomes accordingly larger. It could be seen in the experiments that even if a droplet was immobilized at the end of a rail, it was removed by the next arriving droplet and was released towards the exit port on the right (Fig. 4c). This allows one to generate, by carefully adjusting the trapping strength, a threshold generator, letting pass only droplets above a particular size or a logic AND gate for droplets.

A great advantage of using the photovoltaic effect to manipulate droplets lies in the fact that the virtual rails or barriers are reconfigurable, since the previous light-induced electric field modulation can be erased using homogeneous illumination. Figure 4d shows the droplet movement after the virtual rail has been erased with incandescent microscope illumination, which has the advantage of a broadband spectrum, and hence no speckle noise. In principle, the same effect could be achieved with homogeneous laser illumination. The reason this light source is not used is aesthetic, since speckles always introduce a slight refractive index modulation which is directly visible in the refractive index pattern. For the experiment shown in Fig. 4, it took 45 s for the erasure of the modulation, after which the droplets are no longer guided to the right-hand exit port, but move towards the left-hand exit. Note that this movement is not caused by any residual internal electric fields, but is most likely the result of an obstruction, hence a biased flow. The high volume base stream in this experiment was formed by the insulating TD, so that discharge through the medium conductivity should have a minor influence as compared to the experiment described in Fig. 3. Moreover, it has to be mentioned that the time needed to completely erase the electric fields could be significantly reduced, simply by increasing the intensity of the light source used during this process.

Of course, more complicated structures, such as a droplet splitter or a droplet maze, can easily be induced on the $LiNbO_3$ substrate since the ASLM permits the creation of arbitrary patterns. For example, in Fig. 5 a microfluidic channel is shown where a droplet splitter and a virtual rail are combined, in order to manipulate Novec 7300 droplets in TD. In this experiment, the much thicker as-grown $LiNbO_3$ crystal was used as the bottom substrate, which increases the visibility of the virtual rails in phase-contrast mode. The droplet splitter is positioned at the entrance of the channel and its V-shape allows one to split droplets and route them along different paths: the droplet on the right-hand side naturally moves with the base flow towards the port on the same side of the channel, whereas the droplet on the left-hand side is steered to the same exit

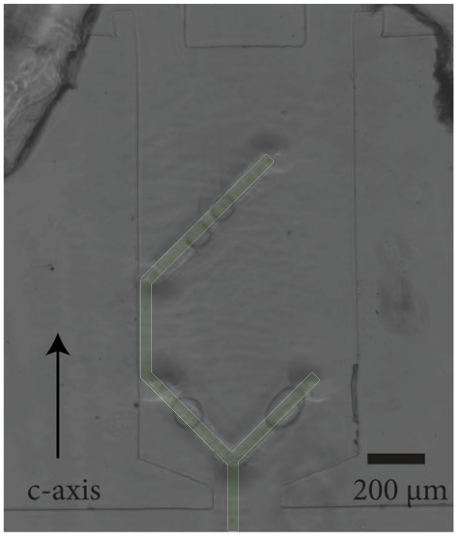

Figure 5 Droplet routing in complex geometries on crystal sample AT2. Novec 7500 droplets flowing TD are split near the droplet nozzle and routed on two different paths as indicated by the green lines. After the splitting, droplets can be merged again in the right-hand output section. Note that in order to visualize the electrode structure, this image has been acquired in Zernike phase-contrast mode. (see video 3: dropletSplittingNovec7500.avi, in online supporting information)

by a follow-up virtual rail. Apart from this proof-of-concept experiment, the possible geometries are only limited by the available output ports and physical space inside the droplet generator.

7. Conclusion and outlook

In this contribution, it was demonstrated how droplets in a microfluidic system can be manipulated and routed only by light, using optically induced evanescent space-charge fields at the surface of an iron-doped $LiNbO_3$ base layer. The origin of the force in the case of uncharged droplets is known as DEP. The structured illumination with a laser through the photorefractive crystal permits the induction of virtual electrodes with arbitrary shapes to control the droplet flow. It has been shown in proof-of-concept experiments that, depending on the electric properties of the combined fluids, this approach enables either repulsion, which has been applied to route bubbles to a certain output port, or attraction, which allows steering on a predefined path inside the microchannel. Due to the size dispersion of the dielectrophoretic and drag forces, it is anticipated that the same mechanism can also be used for sorting applications aiming at the droplet size. Moreover, the possibility of reconfiguring the light-induced structures has been demonstrated, so that the same microfluidic channel can be used for various purposes, such as droplet splitting or mergers. It can be foreseen that due to the very good integrability, the replacement of glass sealing surfaces by $LiNbO_3$ substrates in other droplet synthesis devices is straightforward, leading the way to novel functional devices such as logical droplet operations or adaptive devices, which can dynamically adjust reagent ratios in droplets.

Supporting Information

Additional supporting information may be found in the online version of this article at the publisher's website.

Acknowledgement. The authors are indebted to Cinzia Sada from the Physics and Astronomy Department of the University of Padua for valuable discussions and for supplying lithium niobate samples as well as to Monika Schönhoff from the Department of Chemistry of the University of Münster for conductivity measurements of tetradecane. Financial support from the German Research Foundation (DFG) in the frame of the German-Chinese Transregional Research Cluster TRR61 is gratefully acknowledged. A.Z. further acknowledges financial support from the European Commission in the frame of COST MP1205 and from Fondazione Cassa di Risparmio di Padova e Rovigo (Italy) in the project *Integrated opto-microfluidic prototype on lithium niobate crystals for sensing applications*.

Received: 5 June 2014, **Revised:** 3 November 2014,
Accepted: 20 November 2014

Published online: 18 December 2014

Key words: Optofluidics, Lithium niobate, Droplets, Microfluidics, Photorefractive effect.

References

[1] P. Marcoux, M. Dupoy, R. Mathey, A. Novelli-Rousseaub, V. Heranc, S. Moralesa, F. Riveraa, P. L. Jolya, J. P. Moya, and F. Mallardb, Colloids Surf. A **377**, 54–62 (2011).
[2] I. Shestopalov, J. Tice, and R. Ismagilov, Lab Chip **4**, 316–321 (2004).
[3] Z. Nie, S. Xu, M. Seo, P. Lewis, and E. Kumacheva, J. Am. Chem. Soc. **127**, 8058–8063 (2005).
[4] Z. Nie, W. Li, M. Seo, S. Xu, and E. Kumacheva, J. Am. Chem. Soc. **128**, 9408–9412 (2006).
[5] T. Nisisako, T. Torii, T. Takahashi, and Y. Takizawa, Adv. Mater. **18**, 1152–1156 (2006).
[6] M. Pollack, A. Shenderov, and R. Fair, Lab Chip **2**, 96–101 (2002).
[7] Y. Tan, J. Fisher, A. Lee, V. Cristini, and A. Lee, Lab Chip **4**, 292–298 (2004).
[8] D. B. Wolfe, R. S. Conroy, P. Garstecki, B. T. Mayers, M. A. Fischbach, K. E. Paul, M. Prentiss, and G. M. Whitesides, Proc. Natl Acad. Sci. USA **101**, 12434–12438 (2004), PMID: 15314232.
[9] S. K. Y. Tang, B. T. Mayers, D. V. Vezenov, and G. M. Whitesides, Appl. Phys. Lett. **88**, 061112 (2006).
[10] N. Garnier, R. O. Grigoriev, and M. F. Schatz, Phys. Rev. Lett. **91**, 054501 (2003).
[11] N. T. Nguyen, S. Lassemono, and F. A. Chollet, Sens. Actuators B **117**, 431–436 (2006).
[12] H. Pohl, J. Appl. Phys. **29**, 1182–1188 (1958).
[13] A. Ramos, H. Morgan, N. G. Green, and A. Castellanos, J. Phys. D: Appl. Phys. **31**, 2338–2354 (1998).

[14] R. Pethig, Crit. Rev. Biotechnol. **16**, 331–348 (1996).
[15] S. Fiedler, S. G. Shirley, T. Schnelle, and G. Fuhr, Anal. Chem. **70**, 1909–1915 (1998).
[16] T. B. Jones, J. Electrostatics **51–52**, 290–299 (2001).
[17] P. Chiou, A. Ohta, and M. Wu, Nature **436**, 370–372 (2005).
[18] S. Park, C. Pan, T. H. Wu, C. Kloss, S. Kalim, C. E. Callahan, M. Teitell, and E. P. Y. Chiou, Appl. Phys. Lett. **92**, 151101 (2008).
[19] S. Y. Park, M. A. Teitell, and E. P. Y. Chiou, Lab Chip **10**, 1655–1661 (2010).
[20] H. A. Eggert, F. Y. Kuhnert, K. Buse, J. R. Adleman, and D. Psaltis, Appl. Phys. Lett. **90**, 241909 (2007).
[21] X. Zhang, J. Wang, B. Tang, X. Tan, R. A. Rupp, L. Pan, Y. Kong, Q. Sun, and J. Xu, Opt. Express **17**, 9981–9988 (2009).
[22] M. Esseling, A. Zaltron, C. Sada, and Denz, Appl. Phys. Lett. **103**, 061115 (2013).
[23] M. Esseling, Photorefractive Optoelectronic Tweezers and Their Applications, Springer Theses (Springer, 2014).
[24] S. Glaesener, M. Esseling, and C. Denz, Opt. Lett. **37**, 3744–3746 (2012).
[25] T. Jones, Electromechanics of Particles (Cambridge University Press, 1995).
[26] L. Miccio, M. Paturzo, A. Finizio, and P. Ferraro, Opt. Express **18**, 10947–10955 (2010).
[27] H. Hauser and J. Melcher, Electromagnetic Fields and Energy (Prentice-Hall, 1989).
[28] S. Schmid, C. Hierold, and A. Boisen, J. Appl. Phys. **107**, 054510 (2010).
[29] 3M Deutschland GmbH, Novec 7300 datasheet, November 2013.
[30] 3M Deutschland GmbH, Novec 7500 datasheet, November 2013.
[31] T. Nisisako, T. Torii, and T. Higuchi, Lab Chip **2**, 24–26 (2002).
[32] S. Anna, N. Bontoux, and H. Stone, Appl. Phys. Lett. **82**, 364–366 (2003).
[33] Y. Xia and G. Whitesides, Annu. Rev. Mater. Sci. **28**, 153–184 (1998).
[34] MicroChem, SU-8 negative epoxy series resists, November 2013.
[35] A. del Campo and C. Greiner, J. Micromech. Microeng. **17**, R81–R95 (2007).
[36] A. Glass, D. Linde, and T. Negran, Appl. Phys. Lett. **25**, 233–235 (1974).
[37] K. Buse, J. Imbrock, E. Krtzig, and K. Peithmann, in: Photorefractive Materials and their Application, edited by P. GÃ¼nter and J. Huignard (Springer, 2007), pp. 83–126.
[38] K. Peithmann, A. Wiebrock, and K. Buse, Appl. Phys. B **68**, 777–784 (1999).
[39] M. Esseling, A. Zaltron, N. Argiolas, G. Nava, J. Imbrock, I. Cristiani, C. Sada, and C. Denz, Appl. Phys. B **113**, 191–197 (2013).
[40] N. Kukhtarev, V. Markov, S. Odulov, M. Soskin, and V. Vinetskii, Ferroelectrics **22**, 949–960 (1979).
[41] K. Efimenko, W. Wallace, and J. Genzer, J. Colloid Interface Sci. **254**, 306–315 (2002).
[42] I. Nee, M. Muller, K. Buse, and E. Kratzig, J. Appl. Phys. **88**, 4282–4286 (2000).